RSC Advances

ROYAL SOCIETY OF CHEMISTRY

www.rsc.org/advances

RSC Advances

ARTICLE

Photoinduced electron injection from organic dye having pyridyl anchor to Lewis acid site of TiO_2 surface

Received 00th January 20xx,
Accepted 00th January 20xx

DOI: 10.1039/x0xx00000x

www.rsc.org/

Yutaka Harima,* Yuta Kano, Takuya Fujita, Ichiro Imae, Yousuke Ooyama and Joji Ohshita

An organic dye with a pyridyl group as an anchor unit (**NI4**) adsorbs exclusively on Lewis acid sites of TiO_2 surface although its adsorbability is very weak compared with that of a similar dye with a carboxyl group anchoring to Brønsted acid sites (**NI2**). In the present study, photovoltaic features of the two similar dyes, **NI2** and **NI4**, are investigated deliberately by changing dye loadings on TiO_2 surface and the intensity of illuminated light. A remarkable finding is that photocurrents and photovoltages observed under intense illumination are larger for **NI4** than for **NI2**, suggesting that the adsorbability of dye onto TiO_2 surface is not necessarily a principal factor leading to a high electron injection probability from dye to TiO_2. Plausible reasons for the difference in photovoltaic features between **NI2**- and **NI4**-DSSCs are discussed on the bases of an electrochemical impedance spectroscopy and a transient photovoltage measurements.

1. Introduction

Dye-sensitized solar cells (DSSCs) using nanocrystalline TiO_2 powder and photosensitizing dyes have been studied intensively because of a possible low cost of fabrication and reasonably high power conversion efficiencies.[1-6] A number of studies have been devoted to design and synthesis of efficient photosensitzing dyes and in most of the studies, electron-accepting carboxylic or cyanoacrylic acids have been exclusively employed as an anchor unit to the surface of nanocrystalline TiO_2 particles.[7-10] In contrast to this, we have found that a pyridyl group also acts as an anchoring and electron-withdrawing unit in photosensitizing dyes.[11-15] This finding is of a great importance from a viewpoint that a possible use of a pyridyl anchor can relieve a restriction which has been imposed on design and synthesis of organic photosensitizers for a long time. In our subsequent study, details on adsorption behaviors of an organic dye having a pyridyl anchor (**NI4**) on TiO_2 surface were carefully studied.[16] Analysis of adsorption isotherms for dyes on TiO_2 showed that the adsorption equilibrium constant of **NI4** is two orders of magnitude smaller than that for a similar dye having a carboxyl anchor (**NI2**). In addition, elaborate FT-IR studies with **NI4** powder and **NI4** adsorbed on TiO_2 revealed that a pyridyl dye, **NI4**, adsorbs on Lewis acid sites of TiO_2 in contrast to Brønsted acid sites for a carboxyl dye, **NI2**. Coadsorption experiments with a TEMPO radical (4CT: 4-carboxy 2,2,6,6-tetramethylpiperidine 1-oxyl) and either of **NI2** or **NI4**, coupled with the measurements of average nearest-neighbor interspin distances of 4CT radicals coadsorbed on TiO_2 by a spin-probe ESR technique, supported this view.[16] Currently, a variety of novel anchor units replacing carboxylic (cyanoacrylic) and pyridyl groups have been proposed: cyano-benzoic acid,[17] phosphinic acid,[18] 8-hydroxylquinoline,[19] 2-(1,1-dicyanomethylene)rhodanine,[20] hydroxyl,[21] TCNE and TCNQ,[22] pyradine,[23] benzothienopyridine,[24] and triazine.[25]

It is now of great interest from an academic as well as a practical viewpoint to clarify a relationship between the sort of anchor unit in a photosensitizing dye and the electron injection probability from the dye to TiO_2. Our preliminary study have demonstrated that photocurrents of **NI4**–DSSCs are greater than those of **NI2**–DSSCs when comparisons are made at the same dye loadings on TiO_2 surfaces,[12] although the adsorbability of **NI4** on TiO_2 is much weaker than that of **NI2**. A similar trend was found also for other pyridyl and carboxyl dyes.[13] Up to now, however, detailed studies have not been performed to clarify the reasons for this observation conflicting with a traditional view that a good electron communication between dye and TiO_2 leads to a high electron injection probability. In the present study, photovoltaic properties of DSSCs based on the two similar dyes, **NI2** and **NI4,** are studied carefully by changing dye loadings and the intensity of illuminated light, together with the use of an electrochemical impedance spectroscopy and a transient photovoltage technique.

2. Experimental

2.1. Chemicals. Two kinds of organic dyes **NI2** and **NI4** were synthesized as described earlier[12] and their chemical structures are illustrated in Fig. 1. Tetrahydrofuran (THF, Kanto Chemical Co., Inc.) was purified by distillation and used as solvent for dye adsorption. Acetonitrile (MeCN, Tokyo Kasei) used as solvent for DSSCs was refluxed over P_2O_5 for a couple of hours under N_2 atmosphere. 1,2-

[a] *Department of Applied Chemistry, Graduate School of Engineering, Hiroshima University 1-4-1 Kagamiyama, Higashi-Hiroshima, Hiroshima 739-8527, Japan. E-mail: harima@mls.ias.hiroshima-u.ac.jp; Fax: +81-82-424-5494; Tel: +81-82- 424-6534*

† Electronic supplementary information (ESI) available: Details of CV measurements of the dyes. Absorption spectra of the dyes in a mixed solution. Transient absorption spectroscopy. See DOI:

Dimethyl-3-*n*-propylimidazolium iodide (DMPrII) was obtained from Shikoku Kasei and used as received. 4-*Tert*-butylpyridine (TBP) was from Nacalai Tesque. Other chemicals were used without further purification. The TiO_2 paste (PST-18NR) was purchased from JGC Catalysts and Chemicals Ltd. The fluorine-doped tin oxide (FTO, 13 Ω/□) was obtained from Nippon Sheet Glass Co. Ltd.

2.2. Fabrication of DSSCs and evaluation of dye loadings. In most experiments, two identical dye-adsorbed TiO_2 electrodes were prepared under the same experimental conditions: one was used for photovoltaic measurements and the other for evaluation of dye loading. The TiO_2 paste was deposited on FTO substrate by doctor-blading. The deposited TiO_2 paste was sintered according to a temperature program (from room temperature to 450 °C for 50 min and at 450 °C for 35 min). When the temperature of the TiO_2 electrode was cooled down to 45 °C, the sintered electrode was immersed into THF solutions containing various concentrations of **NI2** or **NI4** in order to control **NI2** or **NI4** loading on TiO_2 surface. Unless otherwise stated, adsorption of **NI2** and **NI4** on TiO_2 was made in THF solutions of 0.2 mM **NI2** and 2 mM **NI4**, respectively, where dye loadings for **NI2** and **NI4** are similar with each other. In all cases, the dye adsorption was performed for 18 hours in an incubator kept at 25 °C. DSSC was fabricated by using one of the two dye-adsorbed TiO_2 electrodes thus prepared, Pt-coated glass as a counter electrode, and a redox solution consisting of 0.05 M I_2, 0.1 M LiI, and 0.6 M DMPrII in MeCN. On the other hand, the other dye-adsorbed TiO_2 electrode was cautiously soaked in pure THF for several seconds and dye loading was determined by taking absorption spectra of a mixed solution (THF:DMSO:H_2O (1M NaOH) = 5:4:1, v:v:v) in which dye molecules deposited on TiO_2 were desorbed for three hours. Time courses of absorption spectra of **NI2** and **NI4** in the mixed solutions are shown in Fig. S1 for demonstrating that both of the dyes are stable in the solutions. The thickness of TiO_2 film (0.5x0.5 cm^2 in photoactive area) was evaluated to be about 9 μm using a 3D-laser scanning microscope (Keyence VK-9700). A specific surface area of the sintered TiO_2 electrode needed for evaluation of dye loadings was determined by N_2 adsorption experiments to be 83 m^2 g^{-1}.

2.3. Photovoltaic measurements. Photocurrent-voltage characteristics of DSSCs were measured with a potentiostat (Hokuto Denko HA-501G) under irradiation of AM 1.5, 100 mW cm^{-2} supplied by a solar simulator (Asahi Spectra HAL-302). Incident photon-to-current conversion efficiency (IPCE) spectra were measured under monochromatic irradiation with a tungsten-halogen lamp (150 W) and a monochromator with intensities of monochromatic lights at different wavelengths measured in advance by use of a thermopile (Eppley Type E6). Dependence of a short-circuit photocurrent (J_{sc}) on light intensity (P) was carefully measured, where a monochromatic light of 410 nm obtained from an interference filter (Toshiba Glass KL-41) and a bandpass filter (Toshiba Glass B390) and a 500-W Xe lamp was used as a light source and its intensity was attenuated using neutral density filters. Intensities of the attenuated 410-nm light were measured using a Si photodiode (Hamamatsu Photonics S1226-5BQ).

2.4. Spectroscopic measurements. Absorption and fluorescence spectra of **NI2** and **NI4** in solutions were taken on a spectrophotometer (Shimadzu UV-3150) and a spectrofluorometer (Hitachi F-4500), respectively.

2.5. Cyclic voltammetry. Cyclic voltammograms (CVs) were recorded in MeCN/TBAP(0.1 M) solution using an air-tight electrolysis cell with a three-electrode system consisting of a Pt sphere as a working electrode, Ag/Ag^+ as a reference electrode, and a Pt wire as a counter electrode. CVs were recorded with a potentiostat equipped with a functional generator (Hokuto Denko HAB-151). Before electrochemical measurements, Ar gas was purged into the electrolyte solution to remove oxygen. Electrode potentials were referred to Ferrocene/Ferrocenium (Fc/Fc^+) redox couple to evaluate HOMO and LUMO energy levels. All the electrochemical measurements were made at room temperature.

2.6. Electrochemical Impedance Spectroscopy (EIS). EIS measurements of DSSCs were performed with an impedance analyzer (VersaSTAT 3, PAR). To measure the impedance, a perturbation amplitude of 10 mV within the frequency range from 10 mHz to 100 kHz was applied in the dark. The observed impedance spectra were analyzed with a software (VersaStudio) to interpret the characteristics of DSSCs.

2.7. Transient photovoltage technique. A light pulse of 0.1 ms duration generated by a light emitting diode (396 nm) was employed in transient photovoltage measurements in the DSSCs. The light pulse was incident on the FTO side of DSSC and its intensity was controlled to keep the change of voltage within 2 mV. White bias light supplied by a halogen lamp (150 W) was also illuminated from the FTO side. The transient photovoltage decay was recorded on an oscilloscope (Iwatsu DS-4372) with an RC circuit (τ = 2.2 s) through a voltage amplifier (NF 5307).

Table 1 Spectroscopic properties of **NI2** and **NI4**, HOMO and LUMO energy levels, and adsorbabilities of **NI2** and **NI4** on TiO_2

Dye	$\lambda_{max}^{abs\,a}$/ nm	$\varepsilon_{max}{}^{a}$/ M^{-1} cm^{-1}	$\lambda_{max}^{fl\,a}$/ nm	$\Phi_f{}^{a,b}$	$E_{1/2}{}^{ox\,c}$/ V	HOMO ^{d}/ V	LUMO ^{d}/ V	K^{e}/ M^{-1}
NI2	376	34300	442	0.87	0.48	1.00	-1.86	0.6×10^5
NI4	375	33000	423	0.84	0.50	1.02	-1.97	1.1×10^3

[a] In 1,4-dioxane. [b] Fluorescence quantum yield determined by a calibrated integrating sphere system (Hamamatsu Photonics). [c] Half-wave potential (*vs.* Ag/Ag^+) for oxidation in MeCN/TBAP(0.1 M). [d] *Vs.* normal hydrogen electrode (NHE). [e] Equilibrium constant for adsorption of the dyes on TiO_2.

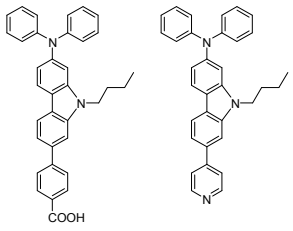

NI2 **NI4**

Fig. 1 Chemical structures of **NI2** and **NI4**.

3. Results and discussion

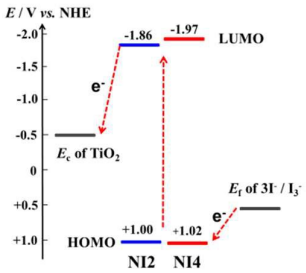

Fig. 2 Energy level diagram of DSSCs based on **NI2** and **NI4**.

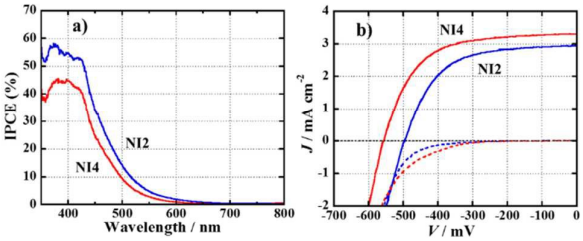

Fig. 3 (a) IPCE spectra and (b) current (*J*)-voltage (*V*) curves of DSSCs based on **NI2** and **NI4**. Solid *J*-*V* curves in Fig. 3b are measured under illumination while broken curves are obtained in the dark.

Spectroscopic and adsorption properties of **NI2** and **NI4** obtained earlier are summarized in Table 1 for the purpose of reference.[12,13,16] Reflecting a similarity of chemical structures except the anchor units between the two dye molecules, absorption and fluorescence wavelengths of the two dyes in 1,4-dioxane are similar with each other. Likewise, CV measurements of the dyes in MeCN showed that both **NI2** and **NI4** exhibit a reversible one-electron transfer process and their redox potentials are close to each other: 0.48 and 0.50 V vs. Ag/Ag^+ for **NI2** and **NI4**, respectively. Details of the CV measurements are given in Supporting Information (Figs. S2-S4). Fig. 2 illustrates the energy level diagram for **NI2**- and **NI4**-DSSCs evaluated with the spectroscopic and electrochemical data of Table 1. A small difference in LUMO energy level is seen between **NI2** and **NI4**. However, the LUMO energy difference of 0.11 eV may not affect the electron injection process in **NI2**- and **NI4**-DSSCs because both the LUMO levels are located sufficiently above the E_c of TiO_2. Likewise, HOMO energy levels of the two dyes are close to each other and well below E_f of the redox couple. These suggest that the combination of **NI2** and **NI4** used in this study can be almost an ideal example for discussing only the difference of the anchor units. On the other hand, there is a marked difference in adsorbability between the dyes: $0.6x10^5$ M^{-1} for **NI2** adsorbed on Brønsted acid sites of TiO_2 and $1.1x10^3$ M^{-1} for **NI4** adsorbed on Lewis acid sites.[16]

Fig. 3 depicts typical IPCE spectra and *J*-*V* curves of DSSCs based on **NI2** and **NI4**, where the dye loadings on TiO_2 (C_{ad}) were $0.99x10^{13}$ cm^{-2} for **NI2** and $0.92x10^{13}$ cm^{-2} for **NI4**. IPCE spectra measured with the same DSSCs as those used in Fig. 3b are similar in shape and the maximum IPCE value at ca. 400 nm is greater for **NI2** than for **NI4**. It is interesting to note in Fig. 3b that the J_{sc} for **NI4** is higher than that for **NI2** in agreement with our previous observation,[12,13] although a larger J_{sc} value should be expected for **NI2** because IPCE values of **NI2** are greater than those of **NI4** over the whole wavelength range. Another salient feature to be noted here is a difference in open-circuit photovoltage (V_{oc}) between **NI4** (560 mV) and **NI2** (500 mV) irrespective of no clear difference in *J*-*V* curves measured in the dark. This photovoltaic feature will be discussed later in detail.

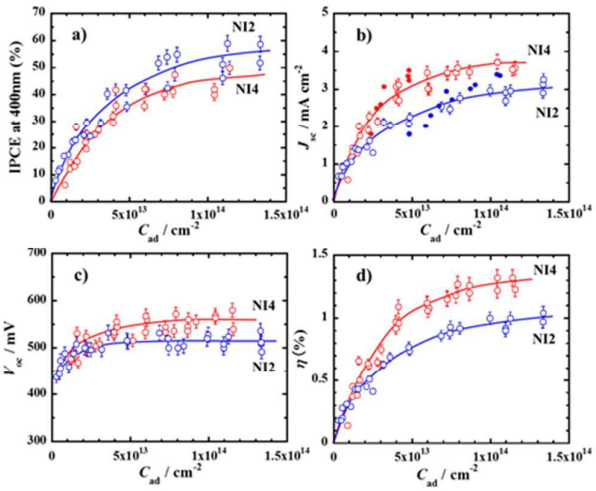

Fig. 4 (a) Plots of IPCE at 400 nm and (b) J_{sc}, (c) V_{oc}, and (d) η against C_{ad} for DSSCs based on **NI2** and **NI4**. Filled circles in blue and red in Fig. 4b denote J_{sc} values for **NI2** and **NI4**, respectively, cited from Fig. 7 of ref. 12,26

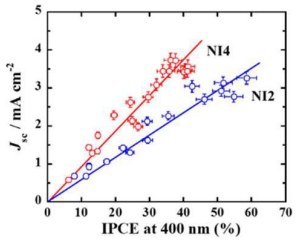

Fig. 5 Correlation between J_{sc} and IPCE at 400 nm for DSSCs based on **NI2** and **NI4**.

In order to make confirmation for the smaller IPCE but greater J_{sc} for **NI4** than those for **NI2**, detailed photovoltaic measurements for **NI2**- and **NI4**-DSSCs were conducted with C_{ad} as a parameter. Fig. 4 summarizes changes of IPCE at 400 nm, J_{sc}, V_{oc}, and energy conversion efficiency (η) with a change of C_{ad}. As is seen in Fig. 4a, IPCE values for both **NI2** and **NI4** increase gradually with the increase of C_{ad} and tend to level off. Over the whole C_{ad} range studied, IPCE values for **NI2** are greater than those for **NI4** in accord with the IPCE spectra of Fig. 3a. Fig. 4b depicts plots of J_{sc} against C_{ad} for **NI2** and **NI4**. Similarly to the plots of IPCE shown in Fig.4a, J_{sc} values for both dyes increase with C_{ad} and tend to saturate. Importantly, however, J_{sc} values for **NI4** are obviously greater than those for **NI2**. This trend of J_{sc} is also consistent with the *J*-*V* curves of Fig. 3b under illumination. We also note that J_{sc} values reported earlier[13] (filled circles in red and blue) do not deviate much from the experimental points obtained in this study. As shown in Fig. 4c, V_{oc} values do not change much with C_{ad} and they are by ca. 50 mV greater for **NI4** than for **NI2** in the high C_{ad} region. Moreover, the values of η calculated with the data of J_{sc}, V_{oc}, and fill factor (*ff*, not shown here because of no obvious difference between **NI2** and **NI4**) as a function of C_{ad} are illustrated in Fig. 4d, which shows higher photovoltaic performances for **NI4** weakly anchoring to Lewis acid sites of TiO_2 than those for **NI2** bonding strongly to Brønsted acid sites.

In what follows, we will discuss intriguing photovoltaic features of DSSCs based on **NI2** and **NI4**. At first, to make the problem

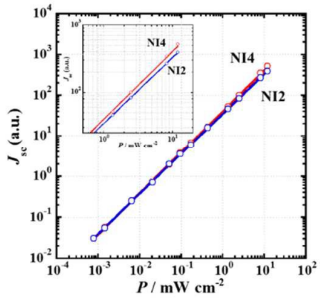

Fig. 6 Double-logarithmic plots of J_{sc} against P for DSSCs based on **NI2** and **NI4**, where illumination is made with a monochromatic light of 410 nm and J_{sc} values at P=0.8 μW cm^{-2} for **NI2**- and **NI4**-DSSCs are equated. Inset denotes a magnified view of the main figure in a high light-intensity regime.

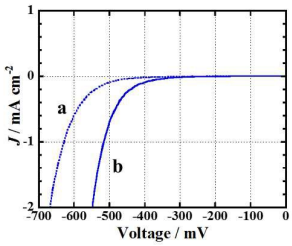

Fig. 7 *J-V* curves of bare TiO_2 electrode in the dark in MeCN/(0.05 M I_2, 0.1 M LiI, and 0.6 M DMPrII) (a) with and (b) without 0.25 M TBP.

clearer, J_{sc} values are plotted against IPCE values at 400 nm, where the data of J_{sc} and IPCE in Figs. 4a and 4b are used in making the plots. It is quite evident from Fig. 5 that the slope of the plot for **NI4** is larger than that for **NI2**. This demonstrates that the photocurrent generation under intense illumination (J_{sc}, white light of 100 mW cm^{-2}) relative to that under weak monochromatic illumination (IPCE, 400-nm light of ca. 1 μW cm^{-2}) is efficient for **NI4** compared with the one for **NI2**. Dependences of J_{sc} on intensity of 410-nm light (P) for **NI2**- and **NI4**-DSSCs were examined over a wide range of P and the results are depicted in Fig. 6 as double logarithmic plots. Here, J_{sc} values observed at the lowest intensity of 0.8 μW cm^{-2} are set equal. Both plots appear to fit straight lines with light exponents (γ in $J_{sc} \propto P^{\gamma}$) almost close to unity over a change in P ranging from ca. 10^{-3} to 10 mW cm^{-2}. When taking a closer look at the high intensity regime shown in the inset of Fig. 6, however, we see that the data points for **NI4** lie slightly above that for **NI2**. This indicates that the recombination loss in photocurrent generation is less enhanced by increasing the light intensity for the case of **NI4** anchoring to Lewis acid sites than for the case of **NI2** anchoring to Brønsted acid sites.

Our second interest in photovoltaic features of **NI2**- and **NI4**-DSSCs is the difference in V_{oc} between **NI2** and **NI4** as illustrated in Figs. 3b and 4c: V_{oc} values for **NI4** are greater than those for **NI2** when compared at the same C_{ad} values. It is well known that the addition of TBP to the electrolyte solution leads to the increase in V_{oc} of DSSC, being sometimes followed by a considerable decrease of J_{sc}.[27-29] The reason for the effect of additive TBP on photovoltaic properties of DSSCs has been discussed to date.[30-32] Currently, the influence of TBP adsorbed on TiO_2 is accounted for in terms of an upward shift of the conduction band of TiO_2 due to the formation of surface dipole layer or a suppression of dark currents by blocking the approach of I_3^- to TiO_2 surface. TBP having a pyridyl group may adsorb on Lewis acid sites of TiO_2 like **NI4**. The influence of TBP is

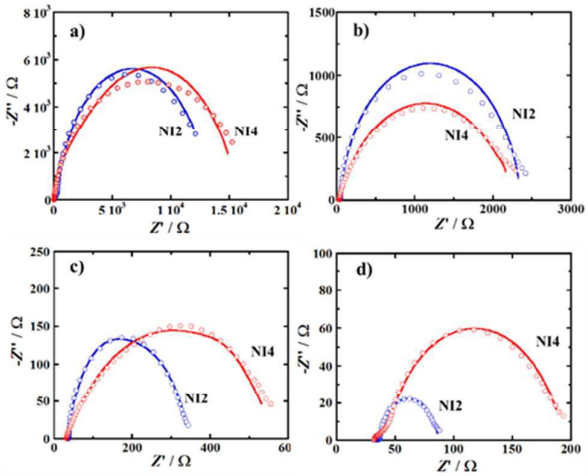

Fig. 8 Nyquist plots and fitting curves of **NI2** and **NI4**-DSSCs biased at a) 300 mV, b) 400 mV, c) 500 mV, and d) 600 mV.

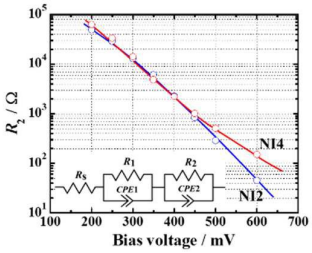

Fig. 9 Charge recombination resistances (R_2) of **NI2**- and **NI4**-DSSCs measured in the dark with the EIS technique. The inset is an equivalent circuit for simulation of DSSCs.

seemingly related to a larger V_{oc} value for **NI4** than for **NI2**. However, it is worth noting that the *J-V* curves in the dark shown in Fig. 3b do not differ much between **NI2**- and **NI4**-DSSCs. In addition, adsorption of **NI2** or **NI4** on the TiO_2 surface did not affect the *J-V* curves observed with the bare TiO_2 electrode although the addition of TBP into electrolyte shifted the *J-V* curve by ca. 100 mV to a negative direction, as shown in Fig. 7. To further investigate properties of the TiO_2 surfaces, EIS measurements of the DSSCs were made and the spectra were simulated as shown typically in Fig. 8, using a simple equivalent circuit shown in the inset of Fig. 9.[33] Here, R_s represents a series resistance due to the sheet resistance of the FTO substrate and electrical contact at FTO/TiO_2 interfaces, R_1 is a charge transfer resistance at the Pt counter electrode, and R_2 denotes a charge-transfer resistance related to recombination of electrons at the TiO_2/electrolyte interface. *CPE*1 and *CPE*2 are constant phase elements corresponding to R_1 and R_2, respectively. Fig. 9 summarizes R_2 values for the **NI2**- and **NI4**-DSSCs measured at various bias voltages in the dark. The R_2 values for the two DSSCs decrease with the increase of the bias voltage with a negligible difference between them except at a bias voltage close to a flat-band potential of the TiO_2 electrodes in contact with the I^-/I_3^- redox solution. These findings demonstrate that the reason for larger V_{oc} values for **NI4** than **NI2** is clearly different from the one for the enhancement of V_{oc} due to the addition of TBP. Moreover, we note that near the flat-band potential of TiO_2, the back reaction of

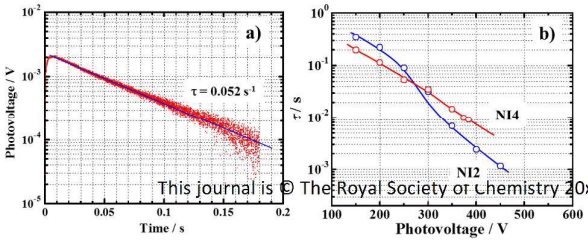

Fig. 10 (a) Typical photovoltage transient signal for **NI4**-DSSC at a photovoltage of 250 mV and (b) electron lifetime (τ) of **NI2**- and **NI4**-DSSCs measured with the transient photovoltage technique.

electrons injected from the LUMO level of the dye into the conduction band of TiO_2 with I_3^- in solution is less probable on the **NI4**-adsorbed TiO_2 electrode than on the **NI2**-adsorbed TiO_2 and this can be responsible for the difference in V_{oc} between **NI2**- and **NI4**-DSSCs. In order to examine this possibility, the transient photovoltage technique was employed to evaluate an electron lifetime in the conduction band (τ) with photovoltage as a parameter.[34,35] A typical photovoltage transient for **NI4**-DSSC is depicted in Fig. 10a and the τ values obtained with the two dyes at different photovoltages are summarized in Fig. 10b. It is seen that the τ values for **NI2**-DSSC are slightly greater than **NI4**-DSSC in the small photovoltage region, whereas they decrease with the increase of the photovoltage and the plots intercept at 250 mV. At higher photovoltages, the electron lifetimes for **NI4**-DSSC are longer than for **NI2**-DSSC, in accord with our speculation that the back electron transfer for **NI4**-DSSC is slow compared with that for **NI2**-DSSC.

More elaborate studies will be needed for in-depth understandings of the mechanisms of charge-injection processes through Brønsted and Lewis acid sites. However, it is now quite clear that the adsorbability of a photosensitizing dye onto TiO_2 surface is not necessarily a principal factor for a high electron injection probability from dye to TiO_2.

4. Conclusions

Photovoltaic features of DSSCs based on **NI4** anchoring weakly to Lewis acid sites of TiO_2 surface are compared with those for **NI2** anchoring strongly to Brønsted acid sites by changing dye loadings on TiO_2 surface. In contrast to a conventional view, it is found that photocurrents observed under illumination of intense light are greater for **NI4** than for **NI2**, although this is not the case under reduced illumination. The finding demonstrates that the adsorbability of a dye on TiO_2 surface is not necessarily a major factor for attaining a high injection probability of electrons from dye to the conduction band of TiO_2. Another feature to be noted for **NI4**-DSSCs is a photovoltage greater than **NI2**-DSSCs. The reason for the difference in photovoltage is ascribed to longer electron lifetimes for **NI4**-DSSCs than **NI2**-DSSCs under intense illumination, on the bases of transient photovoltage measurements and an electrochemical impedance spectroscopy.

Acknowledgements

This work was supported in part by a Grant-in-Aid for Scientific Research (B) (No. 25288085) from the Ministry of Education, Science, Sports and Culture of Japan.

Notes and references

1 N. Robertson, *Angew. Chem., Int. Ed.,* 2006, **45**, 2338-2345.
2 Z. Ning and H. Tian, *Chem. Commun.,* 2009, 483.
3 A. Mishra, M.K.R. Fischer and P. Bäuerle, *Angew. Chem., Int. Ed.,* 2009, **48**, 2474.
4 A. Hagfeldt, G. Boschloo, L. Sun and L. Kloo, *Chem. Rev.,* 2010, **110**, 6595.
5 M. Grätzel, R.A.J. Janssen, D.B. Mitzi and E.H. Sargent, *Nature,* 2012, **488**, 304.
6 K. Kakiage, Y. Aoyama, T. Yano, T. Otsuka, T. Kyomen, M. Unno and M. Hanaya, *Chem. Commun.,* 2014, **50**, 6379.
7 B. O'Regan and M. Grätzel, *Nature,* 1991, **353**, 737.
8 A. Yella, H-W. Lee, H.N. Tsao, C. Yi, A.K. Chandiran, M.K. Nazeeruddin, E.W.-G. Diau, C.-Y. Yeh, S.M. Zakeeruddin and M. Grätzel, *Science,* 2011, **334**, 629.
9 E. Miyazaki, T. Okanishi, Y. Suzuki, Y. N. Ishine, H. Mori, K. Takimiya and Y. Harima, *Bull. Chem. Soc. Jpn.,* 2011, **84**, 459.
10 A.S. Hart, B.K.C. Bikram, N.K. Subbaiyan, P.A. Karr and F. D'Souza, *ACS Appl. Mater. Interfaces,* 2012, **4**, 5813.
11 Y. Ooyama, S. Inoue, R. Asada, G. Ito, K. Kushimoto, K. Komaguchi, I. Imae and Y. Harima, *Eur. J. Org. Chem.,* 2010, 92.
12 Y. Ooyama, S. Inoue, T. Nagano, K. Kushimoto, J. Ohshita, I. Imae, K. Komaguchi and Y. Harima, *Angew. Chem.,* 2011, **50**, 7429.
13 Y. Ooyama, T. Nagano, S. Inoue, I. Imae, K. Komaguchi, J. Ohshita and Y. Harima, *Chemistry-A Euro. J.,* 2011, **17**, 14837.
14 Y. Ooyama, N. Yamaguchi, I. Imae, K. Komaguchi, J. Ohshita and Y. Harima, *Chem. Commun.,* 2013, **49**, 2548.
15 Y. Ooyama, Y. Hagiwara, Y. Mizumo, Y. Harima and J. Ohshita, *New. J. Chem.*, 2013, **37**, 2479.
16 Y. Harima, T. Fujita, Y. Kano, I. Imae, K. Komaguchi, Y. Ooyama and J. Ohshita, *J. Phys. Chem. C.,* 2013, **117**, 16364.
17 M. Katono, T. Bessho, S. Meng, R. Humphry-Baker, G. Rothenberger, S.M. Zakeeruddin, E. Kaxiras and M. Grätzel, *Langmuir,* 2011, **27**, 14248.
18 I. López-Duarte, M. Wang, R. Humphry-Baker, M. Ince, M.K. Martínez-Díaz, M.K. Nazeeruddin, T. Torres and M. Grätzel, *Angew. Chem. Int. Ed.,* 2012, **51**, 1895.
19 H. He, A. Gurung and L. Si, *Chem. Commun.,* 2012, **48**, 5910.
20 J. Mao, N. He, Z. Ning, Q. Zhang, F. Guo, L. Chen, W. Wu, J. Hua and H. Tian, *Angew. Chem. Int. Ed.,* 2012, **51**, 9873.
21 J. Zhao, X. Yang, M. Cheng, S. Li and L. Sun, *ACS Appl. Mater. Interfaces*, 2013, **5**, 5227.
22 T. Michinobu, N. Satoh, J. Cai, Y. Lia and L. Han, *J. Mater. Chem. C,* 2014, **2**, 3367.
23 Y. Ooyama, K. Uenaka, Y. Harima and J. Ohshita, *RSC Adv.,* 2014, **4**, 30225.
24 Y. Ooyama, T. Sato, Y. Harima and J. Ohshita, *J. Mater. Chem. A,* 2014, **2**, 3293.
25 Y. Ooyama, K. Uenaka and J. Ohshita, *RSC Adv.,* 2015, **5**, 21012.
26 Amounts of dye adsorbed on TiO_2 in Fig. 7 of ref. 13 are converted to those for the real TiO_2 surface by using a specific surface area of 83 $m^2 g^{-1}$ for PST-18NR.
27 S.Y. Huang, G. Schlichtho1rl, A.J. Nozik, M. Grätzel and A.J. Frank, *J. Phys. Chem. B,* 1997, **101**, 2576.
28 J. He, G. Benkö, F. Korodi, T. Polıvka, R. Lomoth, B. Åkermark, L. Sun, A. Hagfeldt and V. Sundström, *J. Am. Chem. Soc.,* 2002, **124**, 4922.
29 K. Hara, Y. Tachibana, Y. Ohga, A. Shinpo, S. Suga, K. Sayama, H. Sugihara and H. Arakawa, *Solar Energy Materials & Solar Cells,* 2003, **77**, 89.
30 K. Hara, Y. Dan-oh, C. Kasada, Y. Ohga, A. Shinpo, S. Suga, K. Sayama and H. Arakawa, *Langmuir,* 2004, **20**, 4205.
31 S. Zhang, M. Yanagida, X. Yang and L. Han, *Appl. Phys. Express,* 2011, **4**, 042301/1.
32 J.-Y. Kim, J.Y.; Kim, D.-K. Lee, B. Kim, H. Kim and M.J. Ko, *J. Phys. Chem. C,* 2012, **116**, 22759.
33 L. Yu, K. Fan, T. Duan, X. Chen, R. Li and T. Peng, *ACS Sustainable Chem. Eng.,* 2014, **2**, 718.
34 B.C. O'Regan, I. López-Duarte, M.V. Martínez-Díaz, A. Forneli and J. Albero, *J. Am. Chem. Soc.,* 2008, **130**, 2906.
35 X. Wang, L. Guo, P.F. Xia, F. Zheng, M.S. Wong and Z. Zhu, *J. Mater. Chem. A,* 2013, **1**, 13328.